网络优先出版，实际出版页码及内容以正式版为准

第 55 卷第 8 期 光 子 学 报 Vol.55 No.8
2026 年 8 月 ACTA PHOTONICA SINICA August 2026

引用格式：ZHU Zerui，HONG Ziming，ZHONG Yunxian，et al. Ultra-broadband arbitrary-ratio 1×2 power splitter based on curved inverse tapers[J]. Acta Photonica Sinica，2026，55(8)：0823001
朱泽睿，洪梓铭，仲韵贤，等. 曲线型反向锥超宽带任意比例1×2分光器[J]. 光子学报，2026，55(8)：0823001

曲线型反向锥超宽带任意比例1×2分光器

朱泽睿[1,2,3,5]，洪梓铭[2,3]，仲韵贤[2,3,4]，刘春晓[1*]，何晋平[2,3,4,5*]

（1 南京邮电大学电子与光学工程学院柔性电子（未来技术）学院，南京 210023）
（2 中国科学院南京天文光学技术研究所太阳与空间仪器研究室，南京 210042）
（3 中国科学院天文光学技术重点实验室（南京天文光学技术研究所），南京 210042）
（4 中国科学院大学，北京 100049）
（5 中国科学院大学南京学院，南京 211135）

摘　要：波导阵列集成光子光谱仪因为其优异的性能和紧凑的结构在天文领域受到广泛的关注，但其基于星型耦合器的分光结构在分光数目方面受加工工艺的限制，导致光谱分辨率受限。本文探索其他分光器件的潜在解决方案，其中大带宽、低损耗和分光比高精度可控的任意分光比型1×2分光器是分光元件中的核心结构。本文提出了一种基于曲线型反向锥型的超宽带任意比例1×2分光器，利用亚波长光栅降低了因加工工艺带来的损耗，并通过灵活调节两输出分支的宽度差实现50:50～90:10的任意分光比输出，利用3D FDTD仿真计算得到该类器件在400 nm的工作带宽下可以实现损耗小于0.28 dB且分光比的波动范围小于1.7%。实验结果表明，在1525～1565 nm的带宽范围内损耗小于0.23 dB并且分光比的波动范围小于2.5%。本工作可为任意分光比分光器以及波导阵列集成光子光谱仪的设计与应用提供支撑。

关键词：波导阵列光谱仪；分光器；任意分光比；亚波长光栅；大带宽；低损耗
中图分类号：O436　　　　**文献标识码**：A
doi：10.3788/gzxb20265508.0823001

0　引言

天文光谱观测是获取天体信息的重要手段之一，其中大规模天文光学光谱观测尤为重要，郭守敬望远镜（Large Sky Area Multi-Object Fiber Spectroscopy Telescope，LAMOST）凭借技术创新[1]成为世界上首个发布光谱数突破两千万的巡天项目[2]，远远超过了全世界光谱巡天项目获取的光谱数总和，为天文学家研究银河系及一般星系的形成与演化提供了有力的基础性数据，暗能量光谱巡天望远镜（Dark Energy Spectroscopic Instrument，DESI）首年已获取1500万个遥远天体光谱，是目前规模最大的光谱巡天[3]，该仪器将获取数千万个星系和类星体的光学光谱，构建覆盖近邻宇宙至110亿光年范围的三维地图。随着大规模光谱巡天项目的发展，对单次获取光谱数目的要求在不断提高，下一代光谱巡天装置极大光谱巡天望远镜（Extremely Large Spectroscopic Survey Telescope，ESST）配备光纤数目将超过数万根[4]，升级改造之后的LAMOST配备的光谱仪数目也将提高到150台以上，传统天文光谱仪由于大尺寸、多装置和高造价的特点对大规模光谱巡天的发展带来巨大的挑战，因此集成光子光谱仪引起了人们的关注[5-6]。已经提出的集成光子光谱仪包括，波导阵列型光谱仪，傅里叶变换型光谱仪和单纳米线型光谱仪[7-8]，其中波导阵列光谱仪凭借其高分辨率、高光学效率和大带宽[9]等特点受到了广泛的研究，但由于波导阵列光谱仪的分辨率与波导阵列的

基金项目：国家重点研发计划（2024YFA1612002，2024YFA1612003）；江苏省重点研发计划（BE2023080）；江苏省自然科学基金（BK20251710）
第一作者：朱泽睿，Email：1277342946@qq.com
通讯作者：何晋平，Email：jphe@niaot.ac.cn；刘春晓，Email：chunxiaoliu@njupt.edu.cn
收稿日期：2026-02-13；**录用日期**：2026-06-01

数目N密切相关[10]，传统阵列波导光栅（Arrayed Waveguide Grating，AWG）型光谱仪基于星型耦合器的分光元件受加工工艺的限制，平板波导受应力影响会发生龟裂不能满足更高分辨率的要求（N>200），因此探索其他分光结构成为了新的目标。由于大规模光谱巡天通常需要在尽可能宽的波长范围内获取目标天体的光谱信息，面向暗弱天体的大样本观测，以及需要系统在长时间运行和多通道测量条件下保持良好的响应一致性。因此任意分光比型分光器作为分光结构中的基础器件，在大规模光谱巡天的应用中对它的带宽、损耗以及分光比在工作波段内的稳定性都提出了严格的要求。

近年来，已经提出的任意分光比型分光器包括基于定向耦合器（Directional Coupler，DC）型[11-12]、基于多模干涉耦合器（Multimode Interference，MMI）型[13-15]、基于绝热锥（Adiabatic Tapers）型[16]以及基于Y分支型[17]。其中定向耦合器型和多模干涉耦合器型因为结构简单且易于制造而被广泛应用，但由于对波长的敏感性较高无法保持在大的带宽下任意分光比的稳定输出，并且受制造误差的影响较大限制了其应

用。基于绝热锥型分光器由于要满足绝热条件，通常需要很长的耦合长度，导致器件尺寸较大，并且已经提出的基于亚波长光栅（Subwavelength Grating，SWG）的绝热锥型分光器[18]虽然提高了带宽，但仍无法满足对损耗和分光比稳定性的要求。Y分支型分光器分光原理基于模场的分割受波长的影响较小，但由于加工条件的限制，两分支间的间隙无法做到理想情况下的绝热转换[19]，导致了额外损耗的产生，在已经提出的研究中使用亚波长光栅来减小因为最小特征尺寸带来的影响[20-22]，其中亚波长光栅是指光栅周期远小于工作波长的一种周期性结构，在该条件下，高阶衍射模式被抑制或处于截止状态，光场主要以零级模式传播，因此结构整体上可近似等效为均匀介质，其对折射率的可调控性在光子集成电路中受到了广泛的应用[23]。目前，由HAN S T等[24]利用亚波长光栅结合多模干涉耦合器实现了在1260～1680 nm的波段内任意分光比的输出，其中损耗小于0.4 dB，分光比的波动小于5%。SU Y X等[25]设计了一种相变材料结合Y分支实现了在1300～1600 nm波段内的任意分光比的输出，其中损耗小于0.33 dB，分光比的波动小于3.5%。LU M J等[18]利用亚波长光栅和绝热锥的结合实现任意分光比的输出，在实验中验证了1530～1610 nm波段内损耗小于0.82 dB且分光比的波动小于2.5%。当前研究方案虽然都能实现宽带下任意分光比的输出，但仍存在损耗较大和输出分光比稳定性较差的缺点。

为了解决前文所述问题，本文提出了一种分光器在超大带宽下保持低损耗的同时实现任意分光比稳定输出的方案。该方案通过利用亚波长光栅降低传统Y分支损耗的同时，利用两个曲线型反向锥型输出端实现任意分光比的稳定输出。仿真结果表明，所设计器件在1400～1800 nm的超大带宽下可以实现50:50，60:40，70:30，80:20，90:10分光比的稳定输出，其中分光比的波动范围小于1.7%且损耗低于0.28 dB。在实验测试中，该器件在40 nm（1525～1565 nm）波段范围内实现了任意分光比的稳定输出，其中分光比的波动范围小于2.5%并且损耗小于0.23 dB。

1 器件设计与仿真

所提出分光器的原理图如图1所示，该器件工作在300 nm厚的Si_3N_4平台上，上下包层SiO_2厚度都为3 μm。当TE模式偏振光耦合进输入波导后经过输入端锥形波导将模场展宽，利用在长度为L的两过渡直波导段中间插入周期为Λ，占空比为f_i的亚波长光栅来降低TE基模输入时由于加工精度带来的额外损耗。由于受到加工最小特征尺寸的限制，两输出分支间的间隙gap设置为200 nm。为了实现超宽带下任意分光比的输出，两输出分支设计成曲线型的反向锥型结构，其中两分支输入端宽度相同，输出端宽度分别为W_2和W_3，通过控制W_2不变，改变W_3大小实现光场在两分支传输过程中传播常数的逐渐变化，从而实现输出端任意分光比的输出。

本文利用亚波长光栅可以对波导有效折射率进行调控的特性[23]来减小器件的额外损耗，亚波长光栅的等效折射率可以近似表示为：

$$n_{\mathrm{SWG}}^2 = f \cdot n_{\mathrm{Si_3N_4}}^2 + (1-f) \cdot n_{\mathrm{SiO_2}}^2 \tag{1}$$

式中n_{SWG}为亚波长光栅的等效折射率；f为亚波长光栅的占空比。由式（1）可知可以通过调控占空比来控制亚波长光栅的等效折射率。传统Y分支由于加工工艺水平的限制，两分支间的间隙不能做到绝热转换，导致有效折射率的突变产生额外损耗，本文利用参考文献[20]所示，通过设计占空比逐渐减小的亚波长光栅

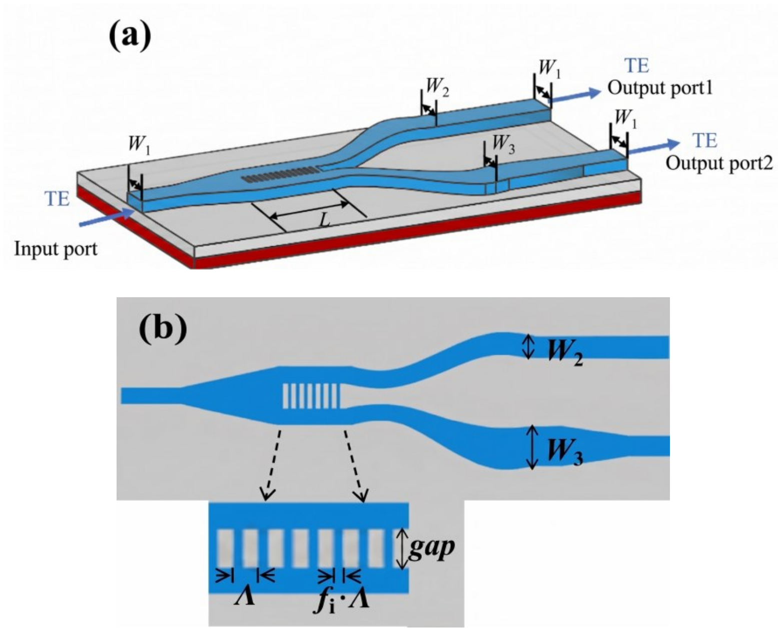

图1　所提出分光器的结构示意图。(a)3D示意图;(b)2D示意图

Fig. 1　Structural schematics of the proposed beam splitter. (a)3D schematic;(b)2D schematic

等效为折射率逐渐降低的介质波导,从而减小模式传播过程中有效折射率的变化,其中亚波长光栅的占空比设计为:

$$f_i = (f_{max} - f_{min}) \cdot \frac{n-i}{n-1} + f_{min} \tag{2}$$

式中f_{max}为最大占空比;f_{min}为最小占空比;n为光栅的阶数。为了分析不同参数对所设计的亚波长光栅性能的影响,采用三维有限差分时域法(3D Finite-Difference Time-Domain, 3D FDTD)进行仿真,使用IL来评价分光器的性能:

$$IL = -10\log_{10}(T_{output1} + T_{output2}) \tag{3}$$

式中$T_{output1}$和$T_{output2}$分别为两个输出端口的透射率。

为了满足单模传输条件,通过模式分析确定单模波导的尺寸为1 μm×0.3 μm。设置输入波导的宽度W_1为1 μm,均匀占空比为f=0.5,耦合长度L=5 μm,在1400~1800 nm波段内模拟了光栅周期与损耗的关系如图2(a)所示。可以从图中看出损耗随着光栅周期的减小而减小,为了满足实际加工条件本文选择Λ=400 nm。在Λ=400 nm的条件下,模拟了不同均匀占空比与损耗的关系如图2(b)所示,随着占空比的减小损耗也在逐渐降低,为了满足最小特征尺寸的要求本文选择f=0.5。

接着将仿真得到的最优均匀占空比f=0.5作为式(2)中的f_{max},接下来讨论渐变占空比对损耗的影响,将f_{min}从0.2到0.4进行了仿真,得到的结果和均匀占空比的对比如图2(c)所示,可以看到渐变占空比的损耗小于最佳均匀占空比,并且随着占空比最小值的减小损耗也在逐渐减小,最后本文选择f_{min}=0.3。根据得到的周期和占空比的结果,对两过渡直波导段的耦合长度L进行了优化,如图2(d)所示最佳耦合长度L=5 μm。

为了获得任意分光比的输出本文定义两个曲线型反向锥的末端宽度差为:

$$\Delta W = W_3 - W_2 \tag{4}$$

式中W_2和W_3分别为两曲线型反向锥的末端宽度,通过改变ΔW产生结构的不对称性实现任意分光比的输出,其中本文将光功率分配器的分光比定义为:

$$PSR = \frac{T_{output2}}{T_{output1} + T_{output2}} \tag{5}$$

式中$T_{output1}$和$T_{output2}$分别为两个输出端口的透射率。

1550 nm下ΔW与两通道输出光强的关系如图3所示,可以看到随着ΔW的变化两通道输出光的强度发

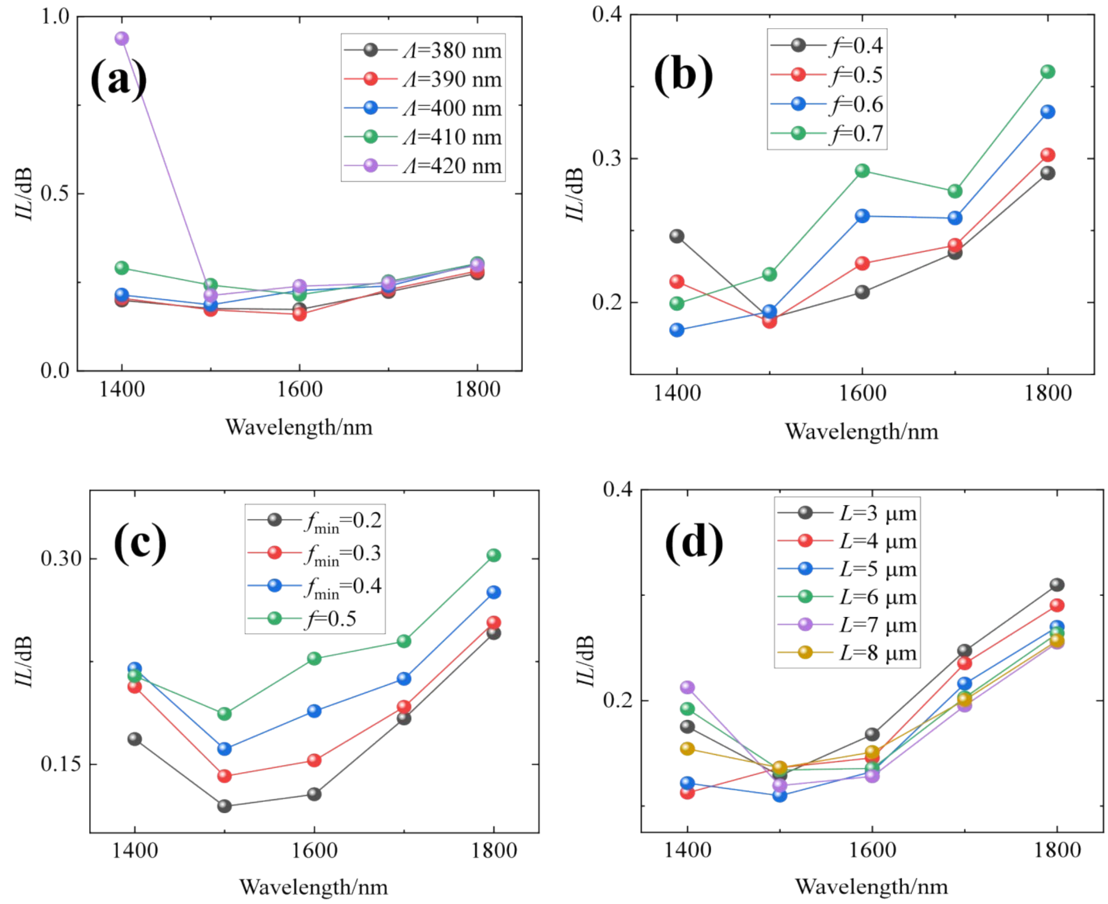

图2 亚波长光栅参数优化。(a)不同光栅周期下的损耗;(b)不同占空比下的损耗;(c)渐变占空比与损耗的关系;(d)不同耦合长度下的损耗

Fig. 2 Optimization of the subwavelength grating parameters. (a) The relationship between the loss and the grating period; (b) the relationship between the loss and the duty cycle; (c) the relationship between the apodized duty cycle and the loss; (d) the relationship between the loss and the coupling length

生了明显的变化,可以实现预期的任意分光比的输出。接着本文分别设计了50:50,60:40,70:30,80:20,90:10分光比下的ΔW,其中60:40和70:30两种分光比的光场传输图像如图4所示,并在1400~1800 nm带宽下仿真了分光比和损耗与波长的关系如图5所示。可以看到在1400~1800 nm的超大带宽下,不同分光比分光器的IL小于0.28 dB且PSR在400 nm带宽下的波动范围小于1.7%。

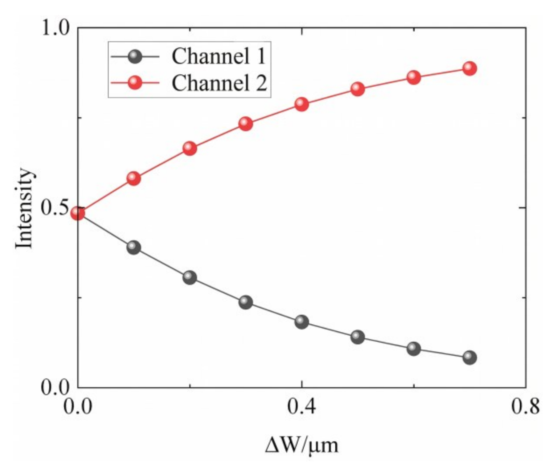

图3 ΔW与两通道输出强度的关系

Fig. 3 Output intensities of the two channels as a function of ΔW

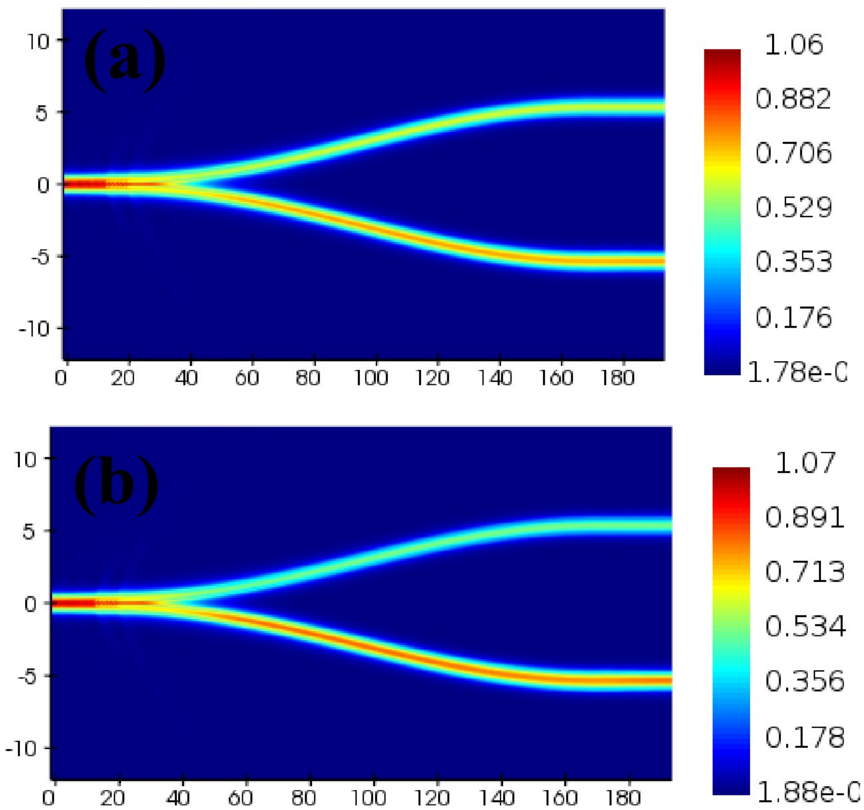

图4　不同分光器的光场传输图样。(a)60:40分光器光场传输图样;(b)70:30分光器光场传输图样

Fig. 4　Optical field propagation profiles of beam splitters with different splitting ratios. (a) 60:40 beam splitter; (b) 70:30 beam splitter

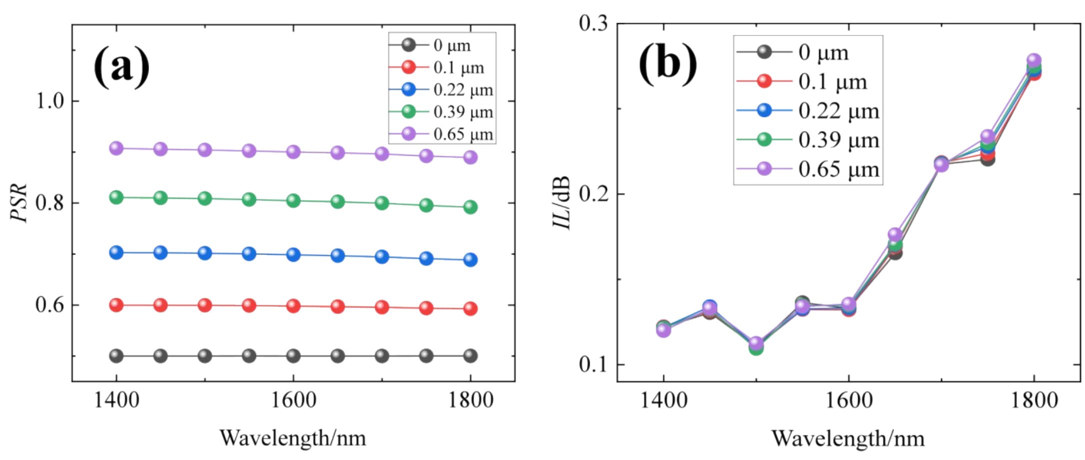

图5　器件宽带性能的仿真计算。(a)分光比与波长的关系;(b)损耗与波长的关系

Fig. 5　Simulation results for the broadband performance of the device. (a) The relationship between the splitting ratio and wavelength; (b) the relationship between the loss and wavelength

2　器件制备与实验测试

为了验证所提出分光器件的可行性,本研究实际加工出样片并对其开展性能研究。本研究在底部厚度为3 μm的氧化层上沉积了300 nm厚的Si_3N_4薄膜,接着采用电子束曝光和电感耦合等离子体刻蚀的方式分别制备了ΔW为0 μm、0.1 μm、0.22 μm、0.39 μm和0.6 μm的分光器。制备好的器件在扫描电子显微镜(SEM)下如图6所示。

实验测试装置如图7所示,光源采用可调谐激光器(Alnair Labs: TLG-220),通过光纤偏振控制器确保

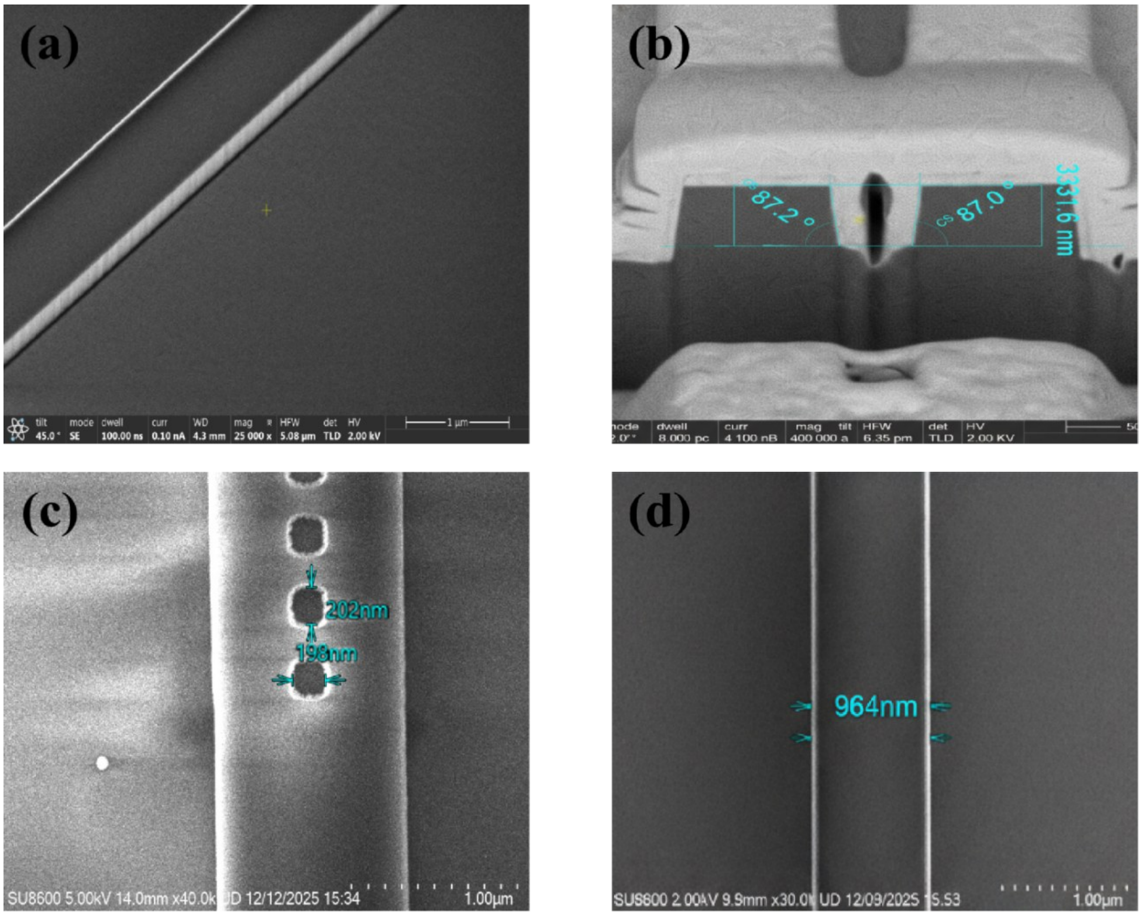

图6　器件的扫描电子显微镜(SEM)图片。(a)波导侧壁的SEM图像;(b)波导刻蚀角度的SEM图像;(c)亚波长光栅区域的SEM图像;(d)单模波导宽度的SEM图像

Fig. 6　Scanning electron microscope (SEM) images of the fabricated device. (a) SEM image of the waveguide sidewall; (b) SEM image of the waveguide etch angle; (c) SEM image of the subwavelength grating region; (d) SEM image of the single-mode waveguide width

输入光为TE模,输入端采用透镜光纤与芯片的端面耦合,输出端采用带有变焦镜头(5～75×)的红外CCD相机(Raptor Photonics:OWL-CL-640)采集输出图像。

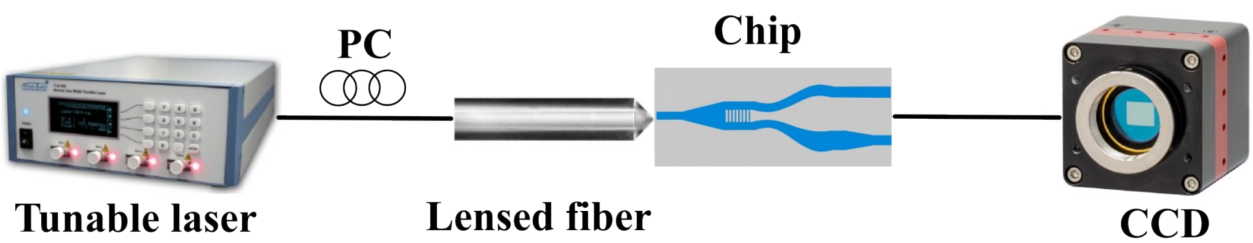

图7　实验测试装置

Fig. 7　Schematic of the experimental setup

为了确保实验的准确性,在最佳耦合位置利用最大放大倍率记录了光场的输出图像,对每个输出通道采用15个大小为15 μm的像素进行采样,以确保每个通道的能量能完整的采集,受实验系统光源带宽的限制,仅在1525～1565 nm波段下进行测试。接着通过在实验中记录没有输入时的图像去除背景噪声带来的影响,将所有采集到的图像进行数据分析。图8显示了1550 nm时分光比为70:30的两个输出通道的强度分布,对两个通道的区域进行积分,事实上两个通道输出的强度之比就是该器件的分光比。接着,使用光功率计测量了光纤端面的输入功率、参考波导端面的输出功率以及每个器件端面的输出功率对器件的损耗进行

了计算。

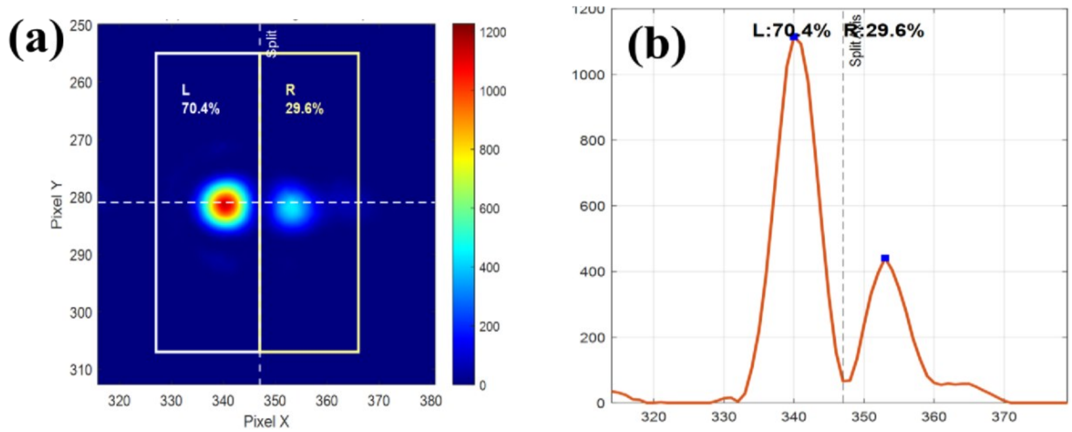

图8 两通道输出光强对比图。(a)去除背景噪声后的输出图像；(b)两个光斑的输出强度分布

Fig. 8 Comparison of the output intensities of the two channels. (a) Output image after removing the background noise; (b) Output intensity profiles of the two optical spots

器件分光比与损耗的实验结果如图9所示，在1525～1565 nm波段下测量的*PSR*波动范围小于2.5%且*IL*小于0.23 dB（仿真计算中该波段*IL*小于0.137 dB），表明该器件可以在较宽的波段范围下工作，然而有部分器件的实验测量的结果与仿真结果有差别，本文认为造成该差异的原因可能是制造过程中加工误差的累积以及实际测量过程中透镜光纤的振动产生的影响。为了验证该观点，本文对该器件的制造公差进行了仿真，考虑到波导的侧壁粗糙度也会对波导的耦合产生影响，为了更好的模拟加工工艺对器件性能的影响，以分光比90∶10为例，给波导的侧壁增加了3 nm的粗糙度，并对波导的宽度增加了±30 nm的误差，如图10所示可以看到加工误差会对实际输出的分光比产生影响，但大部分结果相对集中，以上结果表明，利用现有先进CMOS工艺，所提出的器件具有优良的制造公差。

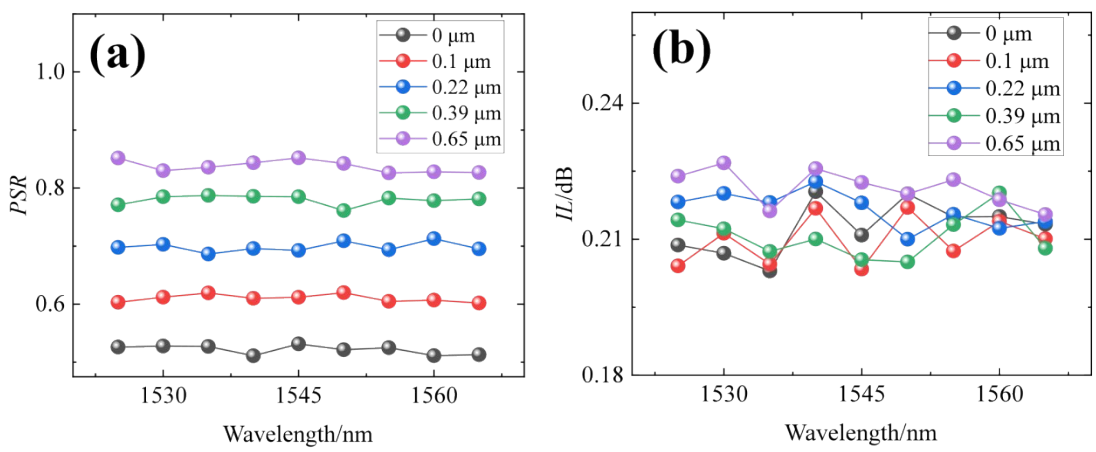

图9 器件分光比与损耗的实验结果。(a)实验测得分光比随波长的变化；(b)实验测得损耗随波长的变化

Fig. 9 Experimental results of the device. (a) The relationship between the splitting ratio and wavelength; (b) The relationship between the loss and wavelength

3 结论

本文设计并实验验证了一种基于曲线型反向锥型的任意分光比型分光器，通过插入亚波长光栅来降低器件因加工工艺带来的损耗，并通过两个宽度不同的曲线型反向锥型波导实现任意分光比的输出。理论上，该器件在1400～1800 nm的波段范围内损耗<0.28 dB，并可以实现50∶50～90∶10的任意分光比的输出且分光比的波动范围小于1.7%。此外，实验结果表明在1525～1565 nm波段内损耗小于0.23 dB且分光比的波动范围小于2.5%，与仿真结果一致。本文所提出器件的宽带特性主要体现在器件的设计及仿真结果，

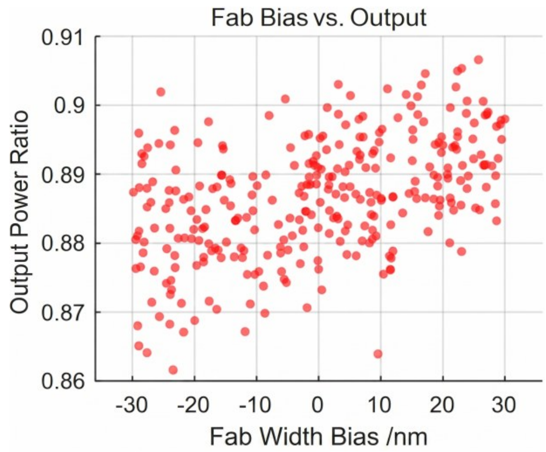

图10 加工误差与分光比的关系

Fig. 10 The relationship between the fabrication error and the splitting ratio

实验部分目前仅在1525～1565 nm波段内进行了验证，实验结果与仿真结果之间的偏差主要与加工误差、耦合不稳定以及测试条件限制有关。后续工作将进一步优化制造工艺与测试平台，并开展更宽波段范围的实验测试，以更全面地验证器件的超宽带工作性能。本文设计的任意比例分光器与的性能与其他参考文献中的分光器的性能比较如表1所示，与已经报道的工作相比，本文提出的基于曲线型反向锥型的任意比例分光器具有大带宽、低损耗和分光比在工作波段内波动较小的特点。此项工作针对传统AWG型光谱芯片在实现高分辨率和大规模分光时，通常依赖较大尺寸的自由传播区，容易受到薄膜残余应力和加工尺寸限制，提供了新型分光结构，后续可以通过级联该结构实现大阵列分光，避免了较大尺寸的自由传播区容易受到薄膜残余应力的问题，该结构在未来波导阵列型集成光子光谱仪的设计、研制及在下一代大规模光谱巡天设施中的应用可提供重要支撑。

表1 1×2任意比例分光器的性能比较

Table1 Performance comparison of 1×2 beam splitters with arbitrary splitting ratios

Structure	Bandwidth/nm	IL/dB	PSR variation	Experimental/Theoretical
SWG－Adiabatic Tapers[18]	400	0.5	5%	Theoretical
	80	0.82	2.5%	Experimental
SWG－MMI[24]	420	0.4	5%	Theoretical
	340	1.5	10%	Experimental
Y－junction[25]	300	0.33	3.5%	Theoretical
MM[14]	300	0.25	3.31%	Theoretical
	35	0.4	8.29%	Experimental
MMI[13]	100	0.2	3%	Theoretical
	70	0.58	4.4%	Experimental
This work	400	0.28	1.7%	Theoretical
	40	0.23	2.5%	Experimental

参考文献

[1] CUI X Q, ZHAO Y H, CHU Y Q, et al. The large sky area multi-object fiber spectroscopic telescope (LAMOST)[J]. Research in Astronomy and Astrophysics, 2012, 12(9): 1197-1242.

[2] https://lamost.org/public/about.

[3] DESI COLLABORATION, AMIROUS P, ANAGNOSTOPOULOS A, et al. Overview of the instrumentation for the dark energy spectroscopic instrument[J]. The Astronomical Journal, 2022, 164(5): 207.

[4] SU D Q, BAI H, YUAN X Y, et al. Optical system for extremely large spectroscopic survey telescope[J]. Science China Physics, Mechanics & Astronomy, 2024, 67(7): 279511.

[5] GATKINE P, VEILLEUX S, HU Y, et al. Arrayed waveguide grating spectrometers for astronomical applications: new results[J]. Optics Express, 2017, 25(15): 17918-17935.

[6] DING Z M, DANG Z Q, JIANG X H, et al. Solar spectrum measured by waveguide spectral lens[J]. Optics & Laser Technology, 2024, 169: 110110.

[7] TONG Xue, LIN Dong, HE Jinping. Current Status of Astro-Photonics Research and Its Application Prospects [J]. Chinese Astronomical Journal, 2022, 63 (05): 26-47.
童雪，林栋，何晋平．天文光子学研究现状及其应用展望[J]．天文学报，2022，63（05）：26-47.

[8] YANG Z Y, ALBROW-OWEN T, CAI W W, et al. Miniaturization of optical spectrometers[J]. Science, 2021, 371 (6528): eabe0722.

[9] HAN Zheng, YUN Binfeng. Design of a Spectral Analysis Chip Based on Cascaded AWGs[J]. Acta Photonica Sinica, 2022, 51(11): 210-219.
韩征，恽斌峰．基于级联AWG的光谱分析芯片设计[J]．光子学报，2022,51(11):210-219.

[10] ZHONG Y X, LIN D, XU B, et al. High-resolution waveguide array-based astronomical spectrograph with cascaded phase modulation[J]. Chinese Optics Letters, 2025, 23(3): 031301.

[11] ZHAO S, LIU W X, CHEN J Y, et al. Broadband arbitrary ratio power splitters based on directional couplers with subwavelength structure[J]. IEEE Photonics Technology Letters, 2021, 33(10): 479-482.

[12] WU H Y, SUN Y H, ZHOU Y, et al. A compact and broadband 2×2 3-dB adiabatic coupler based on trapezoidal subwavelength gratings[J]. IEEE Photonics Journal, 2023, 15(3): 1-6.

[13] ZHAO S, HAN S T, ZHU M Y, et al. Ultra-broadband dual-polarization and arbitrary ratio power splitters based on Bezier curve optimized multimode interference[J]. Optics Letters, 2023, 48(5): 1331-1334.

[14] ZHU Z Z, ZHONG Y X, LIN D, et al. Low-loss and broadband arbitrary ratios 1×2 power splitter based on asymmetrically tapered multimode interference[J]. Journal of Optics, 2024, 26(7): 075801.

[15] DENG Q Z, LIU L, LI X B, et al. Arbitrary-ratio 1×2 power splitter based on asymmetric multimode interference[J]. Optics Letters, 2014, 39(19): 5590-5593.

[16] ZHU J B, QIU C, HUANG H Y, et al. Compact, broadband, and low-loss silicon photonic arbitrary ratio power splitter using adiabatic taper[J]. Applied Optics, 2021, 60(2): 413-416.

[17] LIN Z J, SHI W. Broadband, low-loss silicon photonic Y-junction with an arbitrary power splitting ratio[J]. Optics Express, 2019, 27(10): 14338-14343.

[18] LU M J, GUO Z Z, DENG C Y, et al. Ultracompact and ultrabroadband arbitrary ratio power splitter using subwavelength gratings[J]. Journal of the Optical Society of America B, 2024, 41(3): 685-690.

[19] LOVE J D, RIESEN N. Single-, few-, and multimode Y-junctions[J]. Journal of Lightwave Technology, 2011, 30 (3): 304-309.

[20] ZHOU Y R, YIN C Y, LIU W Y, et al. Design of an ultra-broadband and low-loss 3 dB power splitter from the 1.25 to 2.04 μm wave band[J]. Applied Optics, 2022, 61(32): 9449-9454.

[21] CHEN L, HAN X, ZHOU X D, et al. Demonstration of a high-performance 3 dB power splitter in silicon nitride loaded lithium niobate on insulator[J]. Laser & Photonics Reviews, 2023, 17(11): 2300377.

[22] FERNÁNDEZ DE CABO R, VILAS J, CHEBEN P, et al. Experimental characterization of an ultra-broadband dual-mode symmetric Y-junction based on metamaterial waveguides[J]. Optics & Laser Technology, 2023, 157: 108742.

[23] HALIR R, BOCK P J, CHEBEN P, et al. Waveguide sub-wavelength structures: a review of principles and applications [J]. Laser & Photonics Reviews, 2015, 9(1): 25-49.

[24] HAN S T, SUN D Y, ZHAO S, et al. Ultra-broadband power splitter with arbitrary splitting ratio based on SWG MMI coupler[J]. IEEE Photonics Technology Letters, 2024, 37(3): 137-140.

[25] SU Y X, ZHANG Y R, ZHOU X B, et al. Ultra broadband tunable power splitter based on Sb_2Se_3-assisted Y-junction [J]. Journal of Lightwave Technology, 2023, 42(8): 2817-2822

Ultra-broadband arbitrary-ratio 1×2 power splitter based on curved inverse tapers

ZHU Zerui[1,2,3,5], HONG Ziming[2,3], ZHONG Yunxian[2,3,4], LIU Chunxiao[1*], HE Jinping[2,3,4,5*]

(1 *School of Flexible Electronics (Future Technologies), School of Electronic and Optical Engineering, Nanjing University of Posts and Telecommunications, Nanjing* 210023)

(2 *Solar and Space Instrumentation Laboratory, Nanjing Institute of Astronomy and Optics, Chinese Academy of Sciences, Nanjing* 210042)

(3 *Key Laboratory of Astronomical Optics and Technology, Chinese Academy of Sciences (Nanjing Institute of Astro-*

nomical Optics and Technology), *Nanjing* 210042)
(4 *University of Chinese Academy of Sciences*, *Beijing* 100049)
(5 *University of Chinese Academy of Sciences Nanjing College*, *Nanjing* 211135)

Abstract: Waveguide-array-based integrated photonic spectrometers are widely researched in astronomy for their high performance and compact structure. However, conventional star-coupler-based splitting architectures are restricted by fabrication constraints and film residual stress in thick-film silicon nitride platforms, which limits spectral resolution. High-performance optical power splitter structure, specifically ultra-broadband splitters with low insertion loss and high-precision power controllability, are essential for advanced spectroscopic survey facilities. A curved-inverse-taper-based arbitrary-ratio splitter was designed on a 300-nanometer-thick silicon nitride platform. Subwavelength grating structures were integrated into the coupling region to mitigate excess scattering losses associated with minimum feature size limits in traditional Y-branches. The subwavelength grating was treated as an effective medium with a tunable refractive index governed by the duty cycle. An gradient duty cycle design was applied to transition the effective index linearly, which ensured smooth modal evolution and suppressed back-reflections. The effective refractive index was calculated based on the square root of the weighted average of the dielectric constants of silicon nitride and silicon dioxide. Arbitrary power splitting was achieved by introducing asymmetry in the widths of the curved output branches. Modal propagation constants were tuned by varying the branch width difference, which enabled continuous adjustment of the power splitting ratio from 50:50 to 90:10. To maintain single-mode transmission, waveguide dimensions were constrained to a width of 1 micrometer and a height of 0.3 micrometer. The gap between the two output branches was set to 200 nanometers to comply with standard fabrication limits. Three-dimensional finite-difference time-domain simulations were performed to optimize structural parameters and analyze modal propagation. The subwavelength grating period, the uniform duty cycle, and the coupling length were systematically scanned to identify the minimum loss regime. The optimized configuration utilized a 400-nanometer subwavelength grating period and an gradient duty cycle transitioning from 0.5 to 0.3. A coupling length of 5 micrometers was selected to ensure adiabatic transition. The wavelength range from 1400 to 1800 nanometers was evaluated for ultra-broadband performance. Simulation results show that insertion loss remains below 0.28 decibels across the 400-nanometer bandwidth. The power splitting ratio variation is maintained under 1.7 percent for all investigated ratios, including 50:50, 60:40, 70:30, 80:20, and 90:10. The simulation data confirm that the curved-inverse-taper structure provides superior spectral flatness and wavelength insensitivity compared to conventional multimode interference couplers or directional couplers. Devices were fabricated using electron-beam lithography and inductively-coupled plasma etching. A 300-nanometer-thick silicon nitride film was deposited on a 3-micrometer buried oxide layer. Scanning electron microscopy confirmed the fidelity of the waveguide sidewalls and the high precision of the subwavelength grating patterns. Optical characterization was carried out in the 1525 to 1565 nanometer wavelength range using a tunable laser and an infrared charge-coupled device camera. End-face coupling was facilitated by a lensed fiber. To ensure measurement accuracy, background noise was removed by recording images without laser input. Each output channel was sampled using 15 pixels with a size of 15 micrometers to capture the full mode energy. Experimental results demonstrate an insertion loss under 0.23 decibels and power splitting ratio fluctuation under 2.5 percent. These measurements are consistent with theoretical predictions. Fabrication tolerance was analyzed by simulating the effects of sidewall roughness and width biases on the power splitting ratio of a 90:10 splitter. Discrepancies between simulation and experiment were attributed to a 3-nanometer sidewall roughness and plus or minus 30-nanometer width deviations resulting from the etching process. The curved-inverse-taper arbitrary-ratio splitter combines ultra-broad bandwidth, low loss, and high stability. By cascading this structure to replace the large-area free propagation regions in traditional arrayed waveguide gratings, this architecture provides a potential solution to the film stress issues that typically plague large-scale thick-film devices. The splitter performance remains stable even under significant fabrication biases, suggesting high yield for commercial CMOS foundry processes. This device provides essential technical support for high-resolution integrated spectrometers in next-generation large-scale astronomical spectroscopic surveys.

Key words: Arrayed waveguide spectrometer; Power splitter; Arbitrary splitting ratio; Subwavelength gratings; Broad bandwidth; Low loss

OCIS Codes：130.3120；230.1360；050.6624；350.1260

CSTR：32255.14.gzxb20265508.0823001

Foundation item：National Key R&D Program（2024YFA1612002，2024YFA1612003），Jiangsu Provincial Key R&D Program（BE2023080），Jiangsu Natural Science Foundation（BK20251710）